Biochimica et Biophysica Acta 1808 (2011) 191–198

Contents lists available at ScienceDirect

Biochimica et Biophysica Acta

journal homepage: www.elsevier.com/locate/bbamem

Kinetics of degradation of dipalmitoylphosphatidylcholine (DPPC) bilayers as a result of vipoxin phospholipase A_2 activity: An atomic force microscopy (AFM) approach

Konstantin Balashev [a,d,*], Vasil Atanasov [b], Mariana Mitewa [b], Svetla Petrova [c], Thomas Bjørnholm [d]

[a] Sofia University, Faculty of Chemistry, Department of Physical Chemistry, Lab Biophysical Chemistry, 1, James Bourchier Avenue, Sofia 1164, Bulgaria
[b] Sofia University, Faculty of Chemistry, Department of Analytical Chemistry, Lab Biocoordinational and Bioanalytical Chemistry, 1, James Bourchier Avenue, Sofia 1164, Bulgaria
[c] Sofia University, Faculty of Biology, Department of Biochemistry, Enzymology Lab, 8, Dragan Tsankov Boulevard, Sofia 1164, Bulgaria
[d] Nano-Science Center, Department of Chemistry, University of Copenhagen, Universitetsparken 5, 2100 Copenhagen Ø, Denmark

ARTICLE INFO

Article history:
Received 20 May 2010
Received in revised form 4 October 2010
Accepted 13 October 2010
Available online 17 October 2010

Keywords:
Vipoxin
PLA_2
DPPC bilayers
Enzyme hydrolysis
Atomic force microscopy (AFM)

ABSTRACT

In this paper we used AFM as an analytical tool to visualize the degradation of a phospholipid bilayer undergoing hydrolysis of the vipoxin's PLA_2. We obtained time series images during the degradation process of supported 1, 2-dipalmitoylphosphatidylcholine (DPPC) bilayers and evaluated the occurrence and the growth rate of the bilayer defects. The special resolution of the AFM images allowed us to measure the area and the perimeter length of these defects and to draw conclusions about the kinetics of the enzyme reaction. Moreover, we also report for some unique characteristics discovered during the vipoxin's PLA_2 action. Experimentally for the first time, we observed the appearance and the growth of three-dimensional (3D), crystal-like structures within the formed defects of the degraded bilayer. In an effort to explain their nature, we applied bearing image analysis to estimate the volume of these crystals and we found that their growth rate follows a similar kinetic pattern as the degradation rate of the supported bilayer.

1. Introduction

Phospholipase A_2 enzymes (PLA_2; EC 3.1.1.4) occur ubiquitously in nature and are found in all eukaryotic cell types in pancreatic secretions, inflammatory exudates, snake and arthropod venoms etc. [1]. The secretory PLA_2 (Group II A) are Ca^{2+}-dependent enzymes that catalyze the hydrolysis of the 2-acylester bond of 1, 2-diacyl-3-*sn*-phosphoglycerides. The products of the enzyme reaction—the fatty acids and the lysophospholipids—play important roles in diverse biological processes such as inflammation and signal transduction, remodeling of membrane phospholipids, cell proliferation, and host defense. [1].

The venom of different snakes is one of the natural sources of secreted PLA_2 and in most cases the enzyme is related to the toxicity of the venom complex [2]. Their pharmacological functions involve a variety of effects as neurotoxic, myotoxic, edematogenic, hypotensive, platelet aggregating, cardiotoxic and anticoagulant activities [2].The PLA_2 is also reported to be utilized as a biomarker of pathophysiological processes [3]. The PLA_2s isolated from snake venoms are presented as single-chain proteins (PLA_2 isolated from cobra venoms, ammodytoxins) or as non-covalent ionic type complex, when the enzyme is associated with an acidic and non-toxic component (crotoxin, vipoxin) [2]. The vipoxin's PLA_2 used in this study was isolated from the venom of the Bulgarian long-nose viper *Vipera ammodytes meridionalis*. It is a heterodimeric ionic complex composed of two protein subunits—a basic and strongly toxic His48 phospholipase A_2 and an acidic, enzymatically inactive and nontoxic component. Both subunits have the same polypeptide length (122 amino acid residues) and are closely related, sharing 62% sequence identity. The isolated $sPLA_2$ from vipoxin is one of the most toxic phospholipases (LD100 = 1–3 μg per 20 g mouse, i.v.). When dissociated, the $sPLA_2$ subunit loses its toxicity and enzyme activity in 10–14 days [4–6].

One of the pivotal principles of biochemistry proclaims that deeper knowledge about the kinetic properties of the enzymes leads to better understanding of the mechanisms of their action. In this respect PLA_2 happens to be one of the most studied enzymes [1,7–9]. A well-known fact is that the hydrolytic activity of PLA_2 on aggregated forms of the substrate (micelles, mixed micelles, monolayers, bilayers, liposomes, emulsions etc.) is much higher than the activity on monomolecular dispersions. PLA_2 molecules bind to the substrate interface via enzyme interfacial binding domains which are topologically and functionally separated from the enzyme active site where the catalytic act occurs. The PLA_2 lipolysis is a typical example of heterogeneous catalytic reaction because the enzyme activity strongly depends on the way the substrate molecules are organized [8]. The establishment of the interfacial lipolytic catalysis on monolayers by Verger and de Haas [10] was thoroughly developed by the groups of Verger [11], Panaiotov [12], Brockman [13] and experimentally complemented by variety of advanced physicochemical methods for monitoring the surface activity

* Corresponding author.
E-mail address: kbalashev@chem.uni-sofia.bg (K. Balashev).

0005-2736/$ – see front matter © 2010 Elsevier B.V. All rights reserved.
doi:10.1016/j.bbamem.2010.10.008

of PLA_2. For example, fluorescence microscopy [14], fluorescence spectroscopy [15], electrochemical methods [16], attenuated total reflection Fourier transform infrared (ATR-FTIR) [17], two-photon excitation microscopy [18], light scattering [19], etc., were successfully employed. In the last decade the list of experimental techniques was further extended with the implementation of the atomic force microscopy (AFM). The method has proven its reliability and broad utilization in biology for studying the proteins' structure and enzyme behavior in organized molecular environment that mimics *in vivo* systems [20]. The AFM has two major advantages over any optical microscopic technique: first, it allows the biological surfaces to be imaged with a spatial resolution close to $\approx$1 nm and, second, the occurring changes in the biological species can be followed at high signal-to-noise ratio. As an example, a first direct visual observation of supported bilayer hydrolysis by PLA_2 was reported by Gaub's group [21]. Later on Neilsen et al. showed the existence of a lag-burst kinetics using AFM [22]. It was demonstrated the dependence of the lag time period from the degree of compositional heterogeneity and the number of bilayer defects [23]. Shortly after, Balashev et al. analyzed series of images obtained during the hydrolysis of the supported lipid bilayers as a function of the enzyme concentration and the substrate composition, proving the potential of the AFM as an analytical instrument for study the kinetics of enzyme reactions [24,25].

This article is a step further of the endorsement of the AFM as analytical tool for biological studies. Using the same experimental approach as in refs. [24,25], we visualized the degradation of a bilayer undergoing hydrolysis of the vipoxin's PLA_2. We obtained a time series images during the degradation process of supported 1, 2-dipalmitoylphosphatidylcholine (DPPC) bilayers and evaluated the occurrence and the growth rate of bilayer defects. The special resolution of the AFM images allowed us to measure the area and perimeter length of these defects and to draw conclusions about kinetics of the enzyme reaction. Moreover, we also report for some unique characteristics discovered during the vipoxin's PLA_2 action, which were distinguishable from the earlier reported cases for the lipolysis by PLA_2 observed with the AFM [22,23,25]. We were able to monitor the appearance and the growth of three-dimensional (3D), crystal-like structures within the formed defects of the degraded bilayer. In effort to explain their nature, we applied a bearing image analysis to estimate the volume of these crystals and found that their growth rate follows a similar kinetic pattern as the rate of degradation of the supported bilayer.

2. Materials and methods

2.1. Lipids and other chemicals

1, 2- Dipalmitoyl-*sn*-glycero-3-phosphocholine (DPPC) was purchased from Avanti Polar Lipids (Alabaster, AL). Phospholipid samples were used as received. Other chemicals and salts were purchased from Merck (Germany) or Sigma (Germany). All chemicals and substrates were of analytical grade. We used TRIS buffer (10 mM TRIS-HCl pH 8.0, 0.15 M NaCl and 30 μM $CaCl_2$), which prevents extensive calcium palmitate precipitation and minimizes changes in the Ca^{2+} concentration at the bilayer surface when the negatively charged fatty acid molecules are present. The enzyme concentration used for AFM imaging was 100 nM.

2.2. Isolation of vipoxin's PLA_2

Vipoxin was isolated from crude dried venom of *Vipera ammodytes meridionalis* (Thracian Herpetological Society, Bulgaria) using ion exchange chromatography on SP-Sephadex C-50 (Pharmacia, Sweden) [26]. Vipoxin's PLA_2 was separated by cation exchange chromatography on Mono S HR 5/5 column (Pharmacia) equilibrated with acetate buffer (pH 4.0) in the presence of 6 M carbamide and eluted with a linear gradient of NaCl up to 0.5 M at a flow rate of 0.4 mL/min. The homogeneity of the enzyme was confirmed by SDS-PAGE.

2.3. Enzyme activity assay

The PLA_2 activity of the purified enzyme was measured using synthetic substrate 4-nitro-3-(octanoyloxy) benzoic acid (ONBA) according to the method described by Holzer [27]. The substrate was synthesized using elsewhere published method [28]. The enzyme activity assay was performed by mixing 40 μL of tested PLA_2 solution with 560 μL substrate-containing buffer (250 μL 100 mM $CaCl_2$, 500μL 3 mM ONBA solution in acetonitrile and 5.25 mL of 50 mM TRIS-HCl buffer, pH 8.0; final concentration of the substrate was 0.25 mM). The absorbance was measured at 425 nm using T80+ UV/VIS Spectrometer (UV/TG Instruments), and the initial velocity was calculated (molar absorbance coefficient 5039 mol/L cm in this system). The sample with protein content 230 μg/mL (estimated by bicinchonic acid method [29]) and enzyme activity of 150 μmol/(L mg min) was determined prior the enzyme to be used for further AFM studies.

2.4. Bilayer preparation

The bilayers were formed following the procedure of collapsing small unilamellar vesicles (SUVs) on the supported mica substrate [30,31]. The procedure requires obtaining a suspension of multilamellar vesicles (MLVs). At first the lipid was dissolved in chloroform, and then the solvent was evaporated using rotary evaporator Rotavapor (Buchi, Switzerland) in a thermostatic bath at a temperature 41 °C. As a result a thick lipid film was spread over the wall of the flask. After a further 30 min of drying with argon the lipid in the flask was resuspended in the buffer solution with final lipid concentration of 5 mg/mL. SUVs were obtained from the MLVs by sonication of the suspension to limpidity. During the sonication the MLV suspension was kept in an ice bath. The probe sonicator, Sonicator 3000 (Misonix, Newtown, CT), was set for about 30 min, in pulsed mode at 30% duty cycle. After that the additional centrifugation liposome suspension at 5000×*g* for 20 min is applied in order to be removed the titanium debris emitted by the probe. On freshly cleaved mica discs with diameter of 12 mm (Structure Probe, Inc., SPI Supplies, West Chester, PA), 100μL of newly prepared SUVs were deposited and incubated for 20 min at room temperature. The excess of vesicles was removed by exchanging the solution covering the mica with a buffer and the sample was installed in the liquid cell of the atomic force microscope. The microscope was allowed to thermally equilibrate for a half an hour before imaging.

Two morphological types of bilayer areas were imaged and considered separately. The first type was bilayers with relatively large number of defected areas defined as bilayer holes (Fig. 1A). The second type was bilayers with smaller defects that appeared in the AFM images as surface depressions (Fig. 1B) as their dimensions were comparatively smaller to the size of the AFM tip (Fig. 1D), which could not allow the tip to reach the bottom of the defect (compare Fig. 1C with Fig. 1D).

2.5. AFM imaging

Nanoscope IVa system (Veeco Instruments, Inc.) supplied with a fluid cell was employed for all imaging. A standard silicon O-ring was applied to seal the fluid cell. Prior the imaging the liquid cell was flushed with buffer without enzyme. Cantilevers with oxide-sharpened silicon nitride tips (NanoProbes, Santa Barbara, CA) with a nominal spring constant of 0.06 N m^{-1} were used for scanning. Before enzyme injection the bilayers were equilibrated in the fluid cell for at least 30 min to reduce cantilever drift. All imaging was carried out in contact mode as the force between tip and the sample was maintained manually at a minimum by adjustment of the set point. This approach of force control assures that the loading force is less than 500 pN. The scan rate was 4 Hz

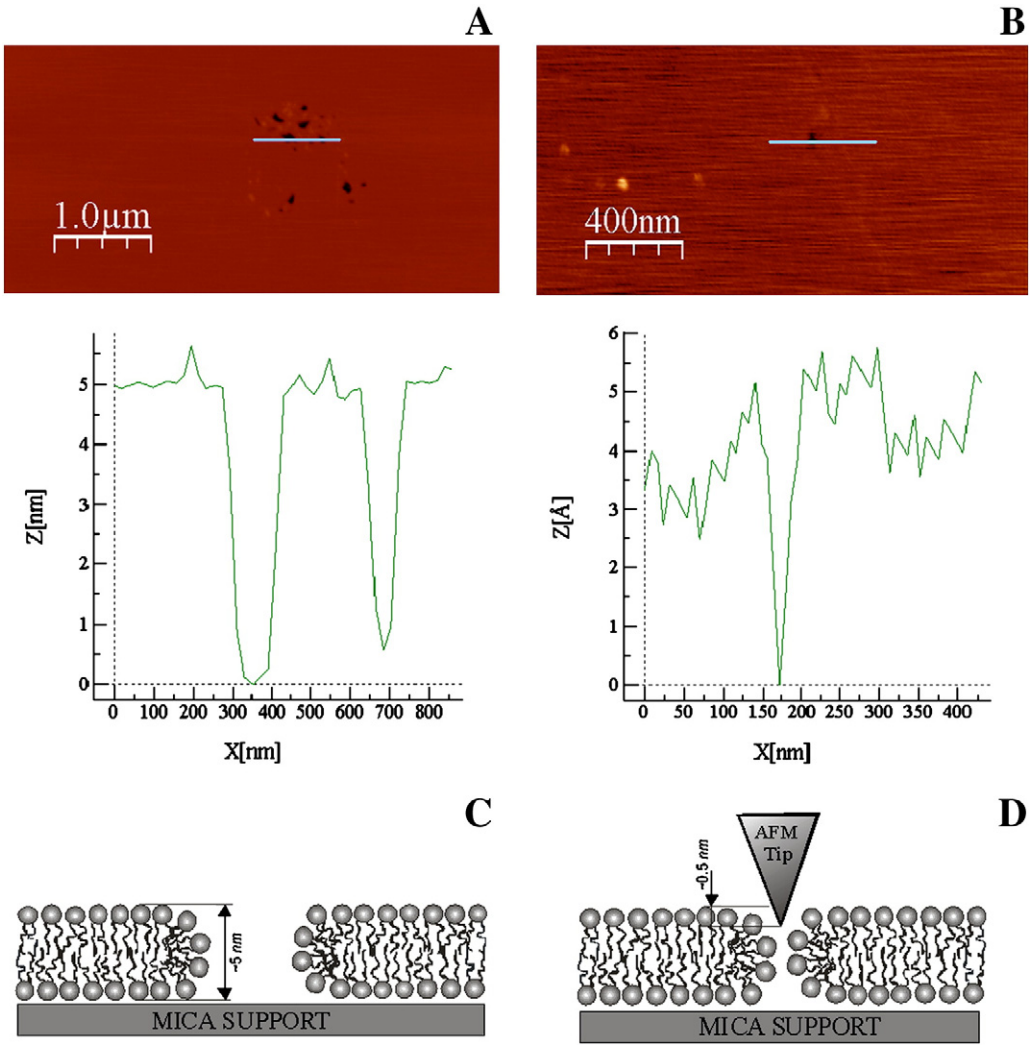

Fig. 1. Two types of imaged bilayer areas. (A) First type is a bilayer with relatively large defected area (holes). The height differences present in the bilayer are a result of the incomplete coverage of the supported mica with phospholipid molecules. The inset shows the profile along the drawn line proving the depth of these holes about 5.0 ± 0.2 nm. (B) Second type of bilayer defects that appeared in the AFM images as small surface depressions. The inset is a profile along the drawn line showing height differences between darker and brighter areas of the bilayer of about 1.0 ± 0.2 nm. (C) A model for the organization of the phospholipid molecules at the edge of the bilayer larger defects. (D) A model for the organization of the phospholipid molecules at the edge of the second type of bilayer defects. These types of defects have dimensions comparable (one order of magnitude) with the size of the AFM tip which prevents the tip to reach the bottom of the defect.

(i.e., 2.1 min/image). To minimize any influence of the tip on hydrolysis, every other frame was scanned with the tip away from the surface except at the very beginning of hydrolysis. Under these conditions, the bilayer can be imaged safely preserving its entity [22–26]. As an additional control, the scan area was increased and/or moved after each experiment to check that hydrolysis had taken place over the entire sample. We found that the extra scanned areas were similar to the previously analyzed, confirming bilayer hydrolysis across the whole sample. This test experiment also assured us that no mechanical impact on the sample within the scanned area has been exerted by the tip. All images have been flattened and corrected for baseline tilt and bow using the Nanoscope software.

2.6. Image analysis

Image analysis was carried out using two public domain programs Scion Image and WSXM 5.0 software packages [32], available on the Internet sites at http://rsb.info.nih.gov/nih-image and http://www.nanotec.es/products/wsxm/download.php, respectively. The bearing analysis for particle volume determination was also performed using the offline version of Veeco software.

3. Results and discussions

Our primary experimental task was to utilize the AFM for characterization of the topography of the supported DPPC bilayers. From the analysis of the obtained AFM images, we quantified the enlargement of the defects (holes) within the scanned bilayer area in the presence of PLA_2. The height differences present in the bilayers (Fig. 1A) were a result of the incomplete coverage of the supported mica and they appeared as holes in the bilayer. When the enzyme is injected into the AFM liquid cell, these bilayer defects started to grow and at some stage of the hydrolysis new holes also appeared. Determining the area fraction of holes in the bilayer at a given time gave a measure of the degree of hydrolysis.

The structural appearance of the supported bilayers once they were transferred into the AFM liquid cell could be characterized as follows (Fig. 1). The total imaged area of all freshly prepared bilayers transferred to the AFM was predominantly composed of a uniformly flat bilayer. Only limited areas (between 0.5% and 5% of the total area) were covered with bilayer defects. We considered two types of bilayer defects. The first type was with relatively large defects (holes) as it shown in Fig. 1A, while the second type were smaller, depression-like

defects (Fig. 1B). The concentration of both types varied between samples as expected from the experimental procedure [30,31]. Nevertheless, for all samples, the defected area fraction never exceeded 5% of the total imaged area. The average depth of the first type of defects was about 5 nm which was in a good agreement with earlier measurements of the thickness of a DPPC bilayer in the gel phase [22–24]. Individual defects had different shapes and sizes and covered areas of less than 0.2 μm^2.

Second types of defects were characterized as small surface depressions about 1 nm in depth relative to the top of the uniform bilayer. These defects appeared as depressions since their lateral size was comparable with the size of the scanning probe. The lateral size of these defects also varied but generally was a factor of 10 smaller than the size of the structural defects. The total area covered by these defects was less than 0.05 μm^2.

It has been repeatedly proven that upon imaging in contact mode with the AFM equipped with a liquid cell, the supported phospholipid membranes in the gel phase remain stable and mechanically intact [22–26]. The performed control experiments for checking the stability and tip-sample interaction effects show no observable changes in the state of imaged DPPC bilayers even during an extensive scanning for a period of 2 h prior to the enzyme injection. In all these test experiments, the imaged bilayers remained stable and undamaged. Subsequently, after a thermal equilibration of the liquid cell for a period of at least 30 min, the enzyme was injected into the cell. The changes of the lipid bilayer structure due to enzyme-induced degradation were followed and image captured over time.

Fig. 2 shows a typical time-course set of images from an experiment prior and after injection of the PLA_2. Few bilayer defects are easily distinguishable at the first image (Fig. 2A) obtained prior to the enzyme

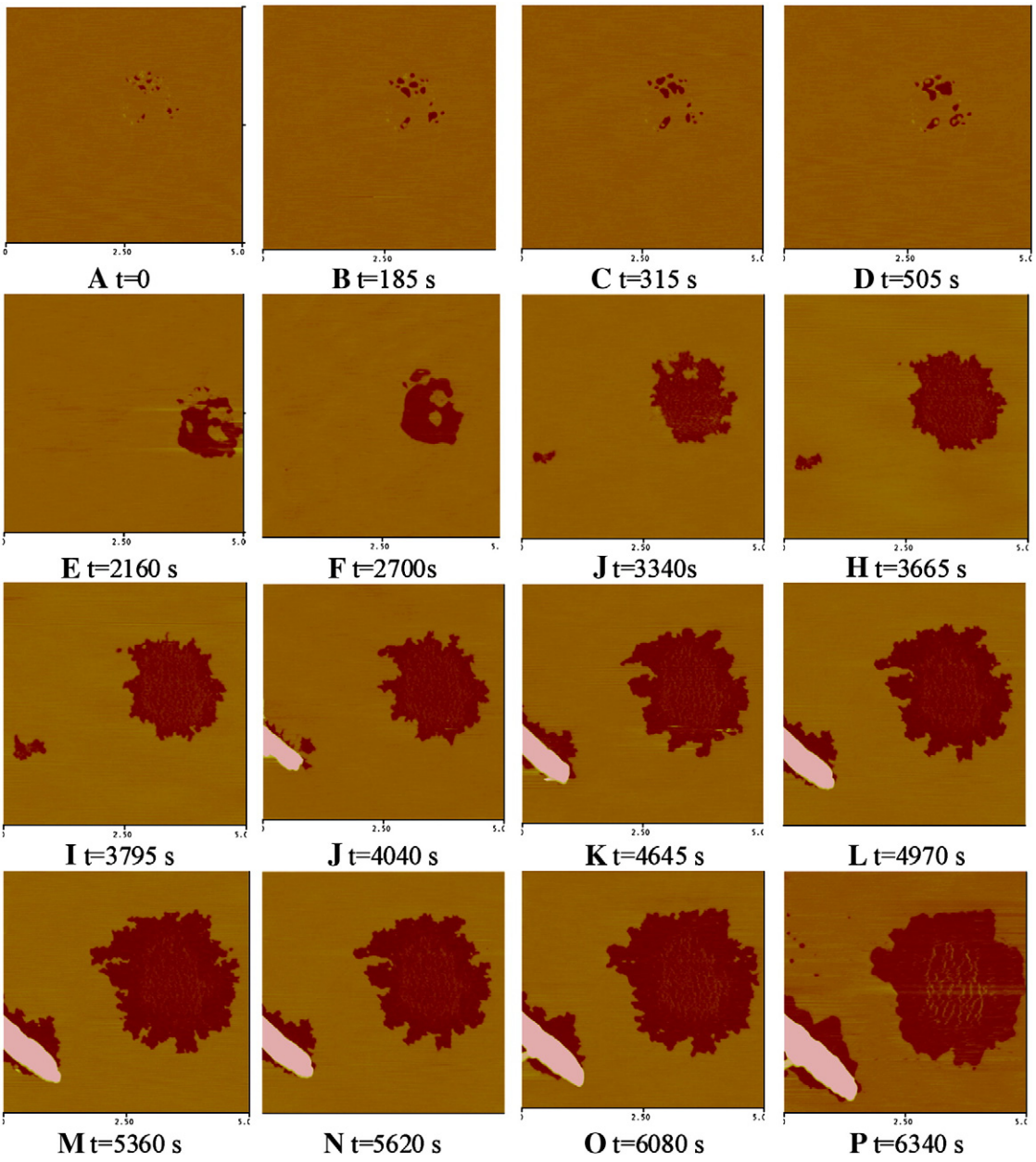

Fig. 2. A typical time-course set of images from an experiment in which 100 nM of vipoxin's PLA_2 solution was injected into the liquid cell (scan size = 5×5 μm^2). Image A is prior to the enzyme injection. The few bilayers defects (darker areas) are easily distinguishable. Image B is captured 185 s. after enzyme injection. The enlargement of the existing defects is necked eye detectable. Images C–P are taken in the time interval 315–6340 s after enzyme injection showing occurrence of progressive changes in surface topology of the bilayer as a result of the enzyme action. The darker areas represent structural defects in the lipid bilayer. After enzyme injection, the initial structural defect expands as the top lipid layer is hydrolyzed and the bottom layer spontaneously desorbs.

injection. The subsequent images (Fig. 2B–P) reveal progressive changes in the surface topology of the bilayer as a result of the enzyme action. We utilized an appropriate software package to analyze the obtained AFM images and estimated the growth rate of these holes. With the PLA_2 present, holes in the bilayer started to grow as a result of hydrolysis of the lipid molecules from the upper layer adjacent to the liquid phase and subsequent desorption of the product molecules-LysoPPC and palmitic acid. Simultaneously DPPC molecules from the bottom layer adjacent to the mica support also desorbed because as soon as the adjoining upper layer "disappears" their hydrophobic tails happened to be exposed unfavorably towards the liquid phase. We measured the area fraction of the bilayer holes as a function of time which gave us a measure of the degree of hydrolysis at various stages of the enzymatic act.

Considering the mechanisms of binding and activation of PLA_2 two already accustomed views should be noted. First, PLA_2 predominantly hydrolyzes bilayer heterogeneous areas of co-existing lipid-lysolipid domains where product accumulation has created phase segregation or the border areas of the existing structural defects because of the loose phospholipid packing at the edge of the holes [25]. Second, PLA_2 hydrolysis is characterized by the existence of a latency period (sometimes referred as a lag time period), i.e., a period of low enzyme activity, followed by a burst [23]. The reaction rate is determined primarily by the properties of the bilayer, i.e., the morphology of the surface, number of defects, etc. Further, we will discuss how our experiments fit in the frame of these views. The very first image (Fig. 2B), obtained about 3 min after the addition of PLA_2 into the liquid cell, clearly shows an increase of the size of already existed defects. Here we underline the fact that primary targets of the enzyme action were only the residing holes in the bilayer. In all experiments no other areas but only the existed membrane structural defects and small bilayer depressions were observed to be affected by the enzyme action. The hydrolyzed areas grow ultimately merging into one common defect. In the course of hydrolysis the appearance of new holes is also observed (Fig. 2P). Fig. 2H shows that the first newly hydrolyzed bilayer area has appeared about 45 min after PLA_2 injection. It was experimentally hard to determine whether these areas of a secondary enzyme attack were phase segregated bilayer domains as the resolution of the obtained images was fairly low when the scanned area was 25 μm^2 or even 9 μm^2. Nevertheless in one occasion about 30 min after the vipoxin injection, we were able to observe the appearance of small depression areas in the bilayer (Fig. 3). These depressions were approximately 0.3–0.5 nm in depth (Fig. 3A). Latter, the emergence of the new bilayer defects as a result of the enzyme action was predominantly within these depression areas (see the arrows in Fig. 3B). These observations confirm the idea that the domains formed in the bilayer during the lag phase are always observed very close to the burst and thus seem to play an important role in the triggering of the burst [22].

In order to quantify the change of the desorbed area and the perimeter length of the existed defects as a function of time, we analyzed the AFM images obtained in the time intervals of about 150 min after PLA_2 injection. A typical result of the kinetics analysis of the growing holes is presented at Fig. 4. The data points obtained from the time series images (Fig. 2A–2P) are presented in a format- desorbed area as a primary ordinate versus time and perimeter length as a secondary *Y*-axis. The locations in the membrane structural defects prior to the enzyme insertion were easily detectable (Fig. 2A). After the PLA_2 solution was injected into the AFM liquid cell the growth of these holes was initiated (Fig. 2B), and it continued until they merged together to form one big bilayer defect (Fig. 2F). As was mentioned previously as a result of the low enzyme activity the appearance of new holes has not

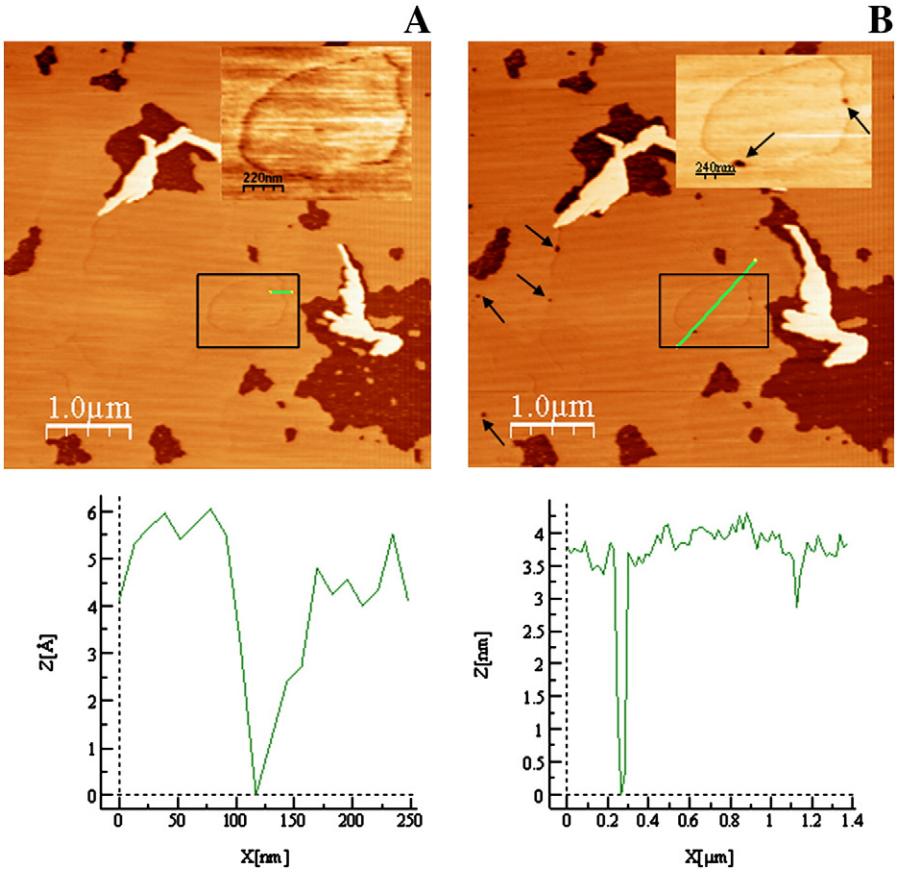

Fig. 3. AFM images obtained after the vipoxin injection showing the appearance of small depression areas in the bilayer (A) 30 min after the vipoxin injection. The inserts show a software zoom of the boxed area with one of several small depression area observed with a typical depth of 0.3–0.5 nm (the *z* scale has been extended to clearly show the depression); also shown is a section through the image; (B) 37 min after the vipoxin injection. Arrows indicate newly appeared defects are presumably created by a single enzyme molecule. Image size, 3 × 3 μm.

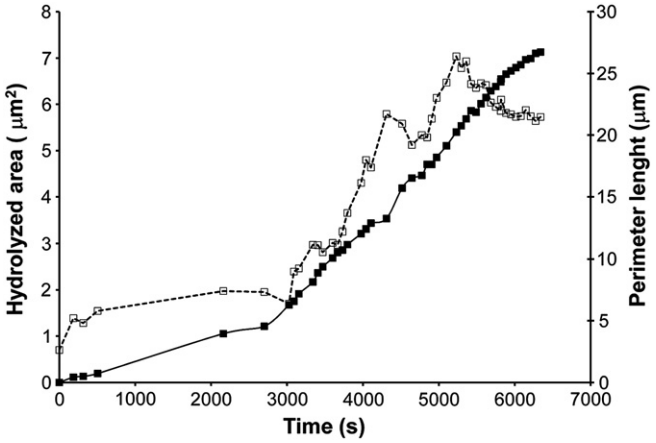

Fig. 4. The change of the hydrolyzed bilayer area and the perimeter length of the existed defects as a function of time. Data points were obtained from the analysis of time series images (Fig. 2A–P) and presented in a format-desorbed area as a primary ordinate versus time (solid curve with filled squares) and perimeter length (dash curve with open squares) as a secondary *Y*-axis. The lag period of this experiment is between 2 and 2.5 times longer than the one reported in ref. [21]. Nevertheless, the two kinetic curves prove the correlation between the hydrolysis rate and the length of the edge of the bilayer defect. When the length of the bilayer edge is large the number of potential spots for the enzyme attack increases.

been observed for some time after the PLA_2 injection into the liquid cell. Once the enzyme was added and the holes were initially formed their number remained the same for relatively long period before the appearance of new bilayer defects. For the different samples this period varied between 40 and 60 min. We assume that, if ever the enzyme binds to the bilayer, it is activated and prefers to "scoot" trough the lipid bilayer. This assumption favors the "scooting mode" as a most realistic molecular model of PLA_2 action [25]. The kinetic curve of the hydrolyzed area versus time shows two distinguishable slopes which corresponded to two regimes of the enzyme hydrolysis. The first one, prior to the appearance of new bilayer defects, was a slow rate hydrolysis while the second one was a burst of the enzyme activity. This kinetic behavior supports the hypothesis for the existence of a lag phase characterized by low enzyme activity, though the lag period measured in our experiments was between 1.5 and 2.5 times longer than the one reported in ref. [22]. The first stage of bilayer hydrolysis occurs preferably at the rims of the existing structural defects and the kinetic curves at Fig. 4 prove the correlation between the hydrolysis rate and the length of the edge of the bilayer defect. The appearance of new holes at the end of the *lag phase* indicated that some other domains of the phospholipid bilayer were also targets of the enzyme attack. As we pointed previously, we can only speculate if these areas were phase separated domains in the bilayer as the microscope resolution did not allow us to study them in close proximity.

In order to further investigate the influence of the initial size of the bilayer defects on the rate of hydrolysis we presented at Fig. 5, two typical data curves obtained for the two morphological types of bilayer areas. First was a bilayer with relatively big number of holes (between 0.05% and 0.5% of the total scanned area) (see Figs. 1A and 2) and second type with smaller number of defects that appeared in the AFM images as small surface depressions (the first image from a typical sequence is shown at Fig. 1B). The defected area in this case was less than 0.05% of the total scanned area. From the kinetic curves at Fig. 5, we distinguished the two regimes of hydrolysis—lag phase and burst. The initial slopes of the curves in the time interval 0–2000 s show that the initial hydrolysis rate in the lag phase was bigger (curve 1) when the bilayer has larger defected area. If we define the initial rate as the hydrolyzed area per time, then the estimation for the initial enzyme activity is $5\times10^{-4}\,\mu m^2/s$, for the bilayer with bigger number of defects (curve 1) and respectively five times smaller $1\times10^{-4}\,\mu m^2/s$ for the bilayer with smaller defective area (curve 2). These values are coherent with the assumption that if bilayer defects are bigger they accommodate at their rim larger number of enzymes and therefore the expected hydrolysis rate is bigger. We can further translate the initial rates by means of the number of DPPC molecules hydrolyzed per second, assuming a mean area per lipid molecule of 0.45 nm^2[21]. As a result we obtain for the initial enzyme activity 1111 DPPC molecules hydrolyzed per second, for the bilayer with bigger number of defects (curve 1) and 222 DPPC molecules hydrolyzed per second, for the bilayer with smaller defective area (curve 2). Further, if we assume that the initial hydrolysis rate was as reported in ref. [20] 88 ± 30 DPPC molecules hydrolyzed/second per enzyme, it would mean that 15 ± 5 (curve 1) and 3 ± 1 (curve 2) enzyme molecules were involved in the initial attack. We can extend this estimate using the available perimeter length of the initial defects- 2.6 μm (curve 1) and 0.226 μm (curve 2). As was reported in [33] the diameter of the vipoxin molecule is about 5.8 nm, which means that the perimeter of the defected area is available for 448 and 40 enzyme molecules respectively seated along the age of the defects in shoulder by shoulder manner. If we compare the last two numbers with the experimentally obtained 15 ± 5 (curve 1) and 3 ± 1, we can conclude that only between 3.3% and 7.5% of the perimeter of the existed bilayer defects are occupied by the enzyme molecules. This result is in a very good agreement with the same obtained in refs. [21, 25]. Once the enzyme reaction steps into the regime where the activity bursts out, the hydrolysis rate has almost the same value for the two morphological types of bilayers and the hydrolysis rate rises up to $20\times10^{-4}\,\mu m^2/s$ (4444 DPPC molecules hydrolyzed per second) (see at Fig. 4 that the slopes of the kinetic curves 1 and 2 are almost the same after $t=2000$ s). It is also observed that when the enzyme reaction steps into the burst stage the growing defects had a finger-like shape with a more profoundly developed channel-like pattern, similar to one previously observed [25].

In this paper we also report for a new phenomenon observed during the process of bilayer degradation—the occurrence and the growth in the course of the enzyme reaction of three-dimensional crystal-like structures. We want to emphasize that these structures appeared in all the occasions only within the frame area of some but not all of the existed defects. As a typical example, from the time image subsequence at Fig. 2J is shown the appearance of such three-dimensional structure at about 1 h and 10 min after PLA_2 injection. In the succeeding images (Fig. 2K–P) the growth of this crystalline structure is easily detectable. Explanation of the nature of this phenomenon provokes some curious

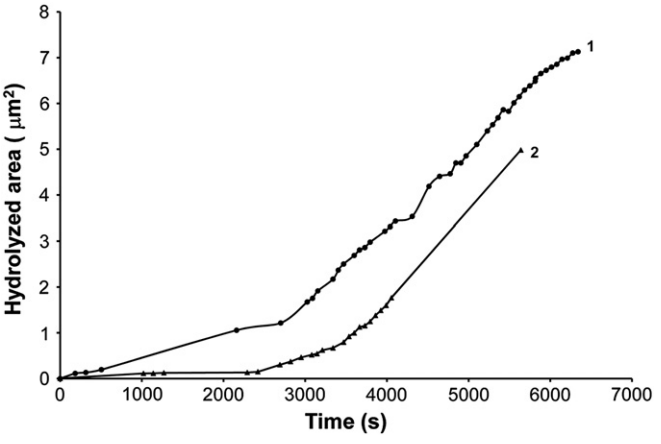

Fig. 5. The change of the hydrolyzed area versus time for the two morphological types of bilayer areas. The two regimes of hydrolysis (lag phase and burst) are easily distinguishable. In the time interval 0–2000 s (lag phase) the initial slop of curve 1 is bigger than the slope of curve 2. If the initial rate is hydrolyzed area per time, then the estimation for the initial enzyme activity is $5\times10^{-4}\,\mu m^2/s$, for the bilayer with bigger number of defects (curve 1) and respectively $1\times10^{-4}\,\mu m^2/s$ for the bilayer with smaller defective area (curve 2). The hydrolysis rate in the burst regime rises up to the same value of $20\times10^{-4}\,\mu m^2/s$ for the two morphological types of bilayers.

questions. As we already mentioned the enzyme hydrolysis leads to product formation and their release from the upper layer adjacent to the liquid and also desorption of unfavorably attached to the mica support phospholipid molecules from the bottom layer. Nevertheless, the concentration of desorbed LysoPPC, palmitic acid and DPPC molecules is estimated to be far below the CMC which would prevent the formation of micelles and their eventual aggregation in 3D structures [24,25]. One explanation of this ambiguity could be hiding in the nature of the vipoxin's PLA_2, which is not very well studied and could play an important part in the molecular aggregation and the growth of these structures. The other could be that the products of the enzyme reaction, LysoPPC and palmitic acid, in addition with desorbed DPPC molecules from the bottom layer which are not affected by the enzyme attack create an organic matrix for the heterogeneous nucleation of the calcium salts [34], thought the low calcium level in the buffer does not favor this hypothesis. In order to avoid more speculations about the intimated nature of these 3D structures, further investigations must be performed with employment of additional experimental methods. Furthermore, we investigated the 3D structures morphology in some close proximity. As an example, Fig. 6 reveals details of the emergence and evolution of a typical crystalline structure. From the presented 3D images and section analysis, one could identify a well-defined sharp-cornered structure, which has number of terraces and a flat plateau forming the top of the structure. Another interesting observation is about the heights of the formed terraces (see for example Fig. 4C): 6 nm, 14 nm and 21 nm. These dimensions coincide with one (5.5 ± 0.5 nm), three (16.5 ± 1.5 nm) and five (22 ± 2 nm) double layer thicknesses, respectively. These sizes support a suggestion that 3D crystalline structures which occurred within the decomposed by the vipoxin's PLA_2 bilayer area, are self organized multilayer structures composed from the lysoproducts of the enzyme reaction and desorbed unhydrolyzed DPPC molecules. Moreover, from the obtained time-course set of images we estimated the growth rate of the 3D structures by measuring their volume. We applied a bearing function analysis available from the Veeco software package in order to estimate the volume of the structures. The graphical results are presented as volume change versus time at Fig. 7 for the two morphological types of bilayer areas. As it appears from the images, during the lag phase of the enzyme reaction, no 3D crystalline structures were observed. Their appearance started at about the same time when the lag-phase period is completed and the

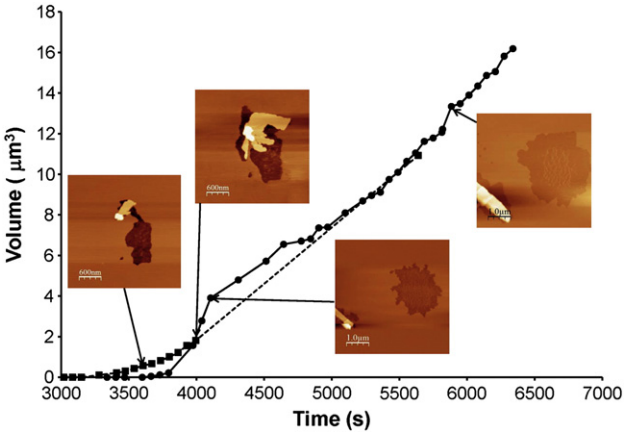

Fig. 7. Two typical curves showing the crystals volume increase versus time. Data points are extracted from two time-course sets of images corresponded for the two morphological types of bilayer areas. Dotted curve with squares corresponds to a bilayer with initially small depression like defects while the solid line with circle points corresponds to a bilayer with initially bigger defects. The example images within the graph frame are presented as the arrows show the data points of the corresponding image. As soon as the first traces of the 3D crystalline structures appeared they started to grow steadily with the volume rate of about 5.5×10^{-3} $\mu m^3/s$.

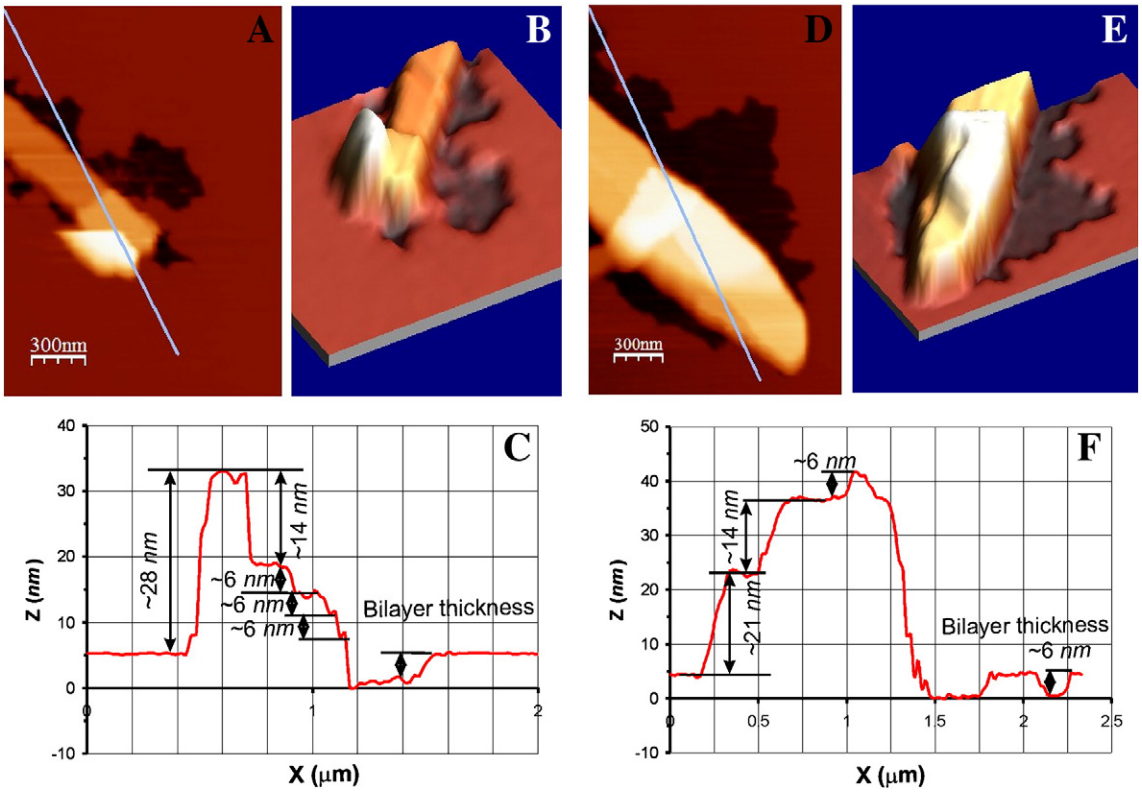

Fig. 6. Images of 3D crystals formed within the lipid bilayer defect during the enzyme hydrolysis obtained approximately (A–C) 4000 s and (D–F) 6000 s after the enzyme injection into the AFM liquid cell. (A) and (D) are the images of the crystals accompanied with the graphs of the cross sections represented at (C) and (F), respectively. (B) and (E) are 3D image views. 3D images and the section analysis show a well defined sharp-cornered structure with number of terraces and a flat plateau forming the top of the structure. The heights of the formed terraces: 6 nm, 14 nm and 21 nm coincide with one (5.5 ± 0.5 nm), three (16.5 ± 1.5 nm) and five (22 ± 2 nm) double layer thicknesses, respectively.

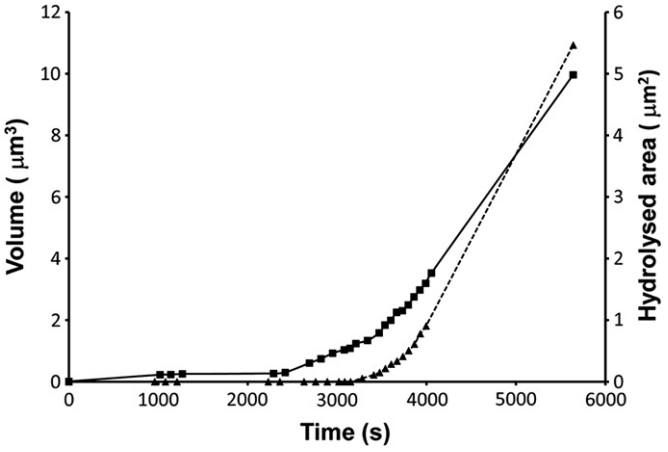

Fig. 8. Comparison between the shapes of the curves—crystals volume versus time (dashed line with triangles) and change hydrolyzed bilayer area (secondary *Y*-axis) as a function of time (solid line with squares).

burst of the enzyme activity is observed. As soon as the first traces of the 3D crystalline structures appeared, they started to grow steadily with the volume rate of about 5.5×10^{-3} μm^3/s. At Fig. 8 the two kinetic curves (3D structures volume change versus time and hydrolyzed bilayer area change as a function of time) are compared. The graph shows that in the time interval 0–3000 s (lag phase) the hydrolyzed area changes slightly because of the low enzyme activity and no 3D structures exist. As soon as the activity bursts out in the time interval after 3000 s, the hydrolyzed area and the volume of the appeared 3D structures start to change following a similar kinetic pattern.

In summary, in this article we made a step further for the utilization of the AFM as an analytical instrument for studying enzyme reactions. We analyzed the time-course images of supported 1, 2-dipalmitoylphosphatidylcholine (DPPC) bilayers undergoing hydrolysis action of Vipoxin's PLA_2 purified from crude dried venom of *Vipera ammodytes meridionalis*. We were able to evaluate the occurrence and the growth rate of two types of bilayer defects. The obtained AFM images allowed us to measure the area and the perimeter length of these defects and to follow their evolution as a result of the enzyme action and also to estimate the initial enzyme activities. Experimentally for the first time we observed the appearance and the growth of three-dimensional (3D), crystal-like structures within the formed defects of the degraded bilayer. We studied the size and the shape of these structures and the kinetic pattern of their growth.

Acknowledgments

This work was supported by the Bulgarian National Fund of Scientific Research (grant DO02-83/12.12.2008) and University of Sofia Science Found (grant SU-181/2009).

References

[1] E.A. Dennis, S.G. Rhee, M.M. Billah, Y.A. Hannun, Role of phospholipase in generating lipid second messengers in signal transduction, FASEB J. 5 (1991) 2068–2077.
[2] R.M. Kini, Phospholipase A_2- a complex multifunctional protein puzzle, in: R.M. Kini (Ed.), Venom phospholipases A_2 Enzymes: Structure, Function and Mechanism, John Wiley & Sons Ltd., New York, 1997, pp. 1–28.
[3] J.N. Swords, Lipoprotein-associated phospholipase A2 novel biomarker and causal mediator of atherosclerosis? Arterioscler. Thromb. Vasc. Biol. 26 (2006) 2417.
[4] B. Aleksiev, B. Tchorbanov, Action on phosphatidylcholine of the toxic phospholipase A_2 from the venom of Bulgarian viper (*Vipera ammodytes ammodytes*), Toxicon 14 (1976) 477–485.
[5] B. Tchorbanov, E. Grishin, B. Aleksiev, Y. Ovchinnikov, A neurotoxic complex from the venom of the Bulgarian viper (*Vipera ammodytes meridionalis*), Toxicon 16 (1978) 37–44.
[6] I. Mancheva, T. Kleinschmidt, B. Aleksiev, G. Braunitzer, Sequence homology between phospholipase and its inhibitor in snake venom The primary structure of the inhibitor of vipoxin from the venom of the Bulgarian viper (*Vipera ammodytes ammodytes*, *Serpentes*), Hoppe-Seyler's Zeitschrift fuer Physiologische Chemie 365 (8) (1984) 885–894.
[7] I. Panaiotov, R. Verger, Enzymatic reactions at interfaces: interfacial and temporal organization of enzymatic lipolysis, in: A.W.N.W. Bazkin (Ed.), Physical Chemistry of Biological Interfaces, Marcel Dekker, New York, 2000, pp. 359–400.
[8] M.K. Jain, G. Berg, The kinetics of interfacial catalysis by phospholipase A_2 and regulation of interfacial activation: hopping versus scooting, Biochim. Biophys. Acta 1002 (1989) 127.
[9] W. Yuan, D.M. Quinn, P.B. Sigler, M.H. Gelb, Kinetic and inhibition studies of phospholipase A2 with short-chain substrates and inhibitors, Biochemistry 29 (1990) 6082–6094.
[10] R. Verger, G. H. deHaas, Enzyme reactions in a membrane model: 1. New technique to study enzyme reactions in monolayers, Chem. Phys. Lipids 10 (1973) 127–136.
[11] R. Verger, G.H. deHaas, Interfacial enzyme-kinetics of lipolysis, Annu. Rev. Biophys. Biol. 5 (1976) 77–117.
[12] M. Ivanova, Tz. Ivanova, R. Verger, I. Panaiotov, Hydrolysis of monomolecular films of long chain phosphatidylcholine by phospholipase A2 in the presence of β-cyclodextrin, Colloids Surf., B 6 (1) (1996) 9–17.
[13] W.E. Momsen, H.L. Brockman, Recovery of monomolecular films in studies of lipolysis, Method Enzymol. 286 (1997) 292–305.
[14] D.W. Grainger, A. Reichert, H. Ringsdorf, C. Salesse, Hydrolytic action of phospholipase A_2 in monolayer phase transition region: direct observation of enzyme domain formation using fluorescence microscopy, BBA Biomembr. 1023 (1990) 365–379.
[15] M.K. Jain, B.P. Maliwal, Spectroscopic properties of the states of pig pancreatic phospholipase A_2 at interfaces and their possible molecular origin, Biochemistry 32 (1993) 11838–11846.
[16] S. Chen, H.D. Abruna, Enzymatic activity of a Phospholipase A_2: an electrochemical approach, Langmuir 13 (1997) 5969–5973.
[17] S.A. Tatulian, Toward understanding interfacial activation of secretory phospholipase A_2 (PLA_2): membrane surface properties and membrane-induced structural changes in the enzyme contribute synergistically to PLA_2 activation, Biophys. J. 80 (2001) 789–800.
[18] S.A. Sanchez, L.A. Bagatolli, E. Gratton, T.L. Hazlett, A two-photon view of an enzyme at work: crotalus atrox venom PLA_2 Interaction with single-lipid and mixed-lipid giant unilamellar vesicles, Biophys. J. 82 (2002) 2232–2243.
[19] P. Høyrup, T.H. Callisen, M.Ø. Jensen, A. Halperin, O. Mouritsen, Lipid protrusions membrane softness and enzymatic activity, Phys. Chem. Chem. Phys. 6 (2004) 1608–1615.
[20] D.J. Muller, AFM: A Nanotool in Membrane Biology, Biochemistry 47 (31) (2008) 7986–7998.
[21] M. Grandbois, H. Clausen-Schaumann, H.E. Gaub, Atomic force microscope imaging of phospholipid bilayer degradation by phospholipase A_2, Biophys. J. 74 (1998) 2398–2404.
[22] L.K. Nielsen, J. Risbo, T.H. Callisen, T. Bjørnholm, Lag-burst kinetics in phospholipase A_2 hydrolysis of DPPC bilayers visualized by atomic force microscopy, BBA Biomembr. 1420 (1998) 266–271.
[23] L.K. Nielsen, K. Balashev, T.H. Callisen, T. Bjørnholm, Influence of product phase separation on phospholipase A_2 hydrolysis of supported phospholipid bilayers studied by force microscopy, Biophys. J. 83 (2002) 2617–2624.
[24] K. Balashev, M. Gudmand, L. Iversen, T.H. Callisen, A. Svendsen, T. Bjørnholm, *Humicola lanuginosa* lipase hydrolysis of monooleoyl-rac-glycerol at the lipid–water interface observed by atomic force microscopy, BBA Biomembr. 1615 (2003) 93–102.
[25] K. Balashev, N.J. DiNardo, T.H. Callisen, A. Svendsen, T. Bjørnholm Atomic, force microscope visualization of lipid bilayer degradation due to action of phospholipase A_2 and *Humicola lanuginosa* lipase, BBA Biomembr. 1768 (2007) 90–99.
[26] B. Tchorbanov, B. Aleksiev, A simple procedure for the isolation of vipoxin- a neurotoxin with weak phospholipase activity from the venom of the Bulgarian viper, J. Appl. Biochem. 3 (1981) 558–561.
[27] M. Holzer, S.P. Mackessy, An aqueous endpoint assay of snake venom phospholipase A2, Toxicon 34 (10) (1996) 1149–1155.
[28] W. Cho, M.A. Markowitz, F.J. Kezdy, A new class of phospholipase A_2 substrates: kinetics of the phospholipase A2 catalyzed hydrolysis of 3-(acyloxy)-4-nitrobenzoic acids, J. Am. Chem. Soc. 110 (1988) 5166–5171.
[29] C.M. Stoscheck, Quantitation of protein, Method Enzymol. 182 (1990) 50–69.
[30] I. Reviakine, Atomic Force Microscopy of Biological Macromolecules and Their Assemblies, Thesis, University of Groningen, Groningen, the Netherlands, November 2000.
[31] I. Reviakine, A. Brisson, Formation of supported phospholipid bilayers from unilamellar vesicles investigated by atomic force microscopy, Langmuir 16 (2000) 1806–1815.
[32] I. Horcas, R. Fernández, J.M. Gómez-Rodríguez, J. Colchero, WSXM: A software for scanning probe microscopy and a tool for nanotechnology, Rev. Sci. Instrum. 78 (2007) 013705.
[33] D.N. Georgieva, N. Genov, K. Hristov, K. Dierks, C. Betzel, Interactions of the neurotoxin vipoxin in solution studied by dynamic light scattering, Biophys. J. 86 (2004) 461–466.
[34] D.M. Sharbaugh, D.R. Talham, Effect of phospholipase A_2 hydrolysis products on calcium oxalate precipitation at lipid interfaces, Langmuir 26 (2010) 4925–4932.